



Article

Multiple Regression Analysis and Non-Dominated Sorting Genetic Algorithm II Optimization of Machining Carbon-Fiber-Reinforced Polyethylene Terephthalate Glycol Parts Fabricated via Additive Manufacturing Under Dry and Lubricated Conditions

Anastasios Tzotzis ^{1,*} , Nikolaos Efkolidis ¹, Kai Cheng ² and Panagiotis Kyratsis ¹ 

¹ Department of Product and Systems Design Engineering, University of Western Macedonia, 50100 Kila Kozani, Greece; nefkolidis@uowm.gr (N.E.); pkyratsis@uowm.gr (P.K.)

² Department of Mechanical and Aerospace Engineering, Brunel University London, Uxbridge UB8 3PH, UK; kai.cheng@brunel.ac.uk

* Correspondence: a.tzotzis@uowm.gr

Abstract: The present research deals with the processing of the additively manufactured Carbon-Fiber-Reinforced Polymer (CFRP) under dry and lubricated cutting conditions, focusing on the generated surface roughness. The cutting speed, feed, and depth of cut were selected as the continuous variables. A comparison between the generated surface roughness of the dry and the lubricated cuts revealed that the presence of coolant contributed towards reducing surface roughness by more than 20% in most cases. Next, a regression analysis was performed with the obtained measurements, yielding a robust prediction model, with the determination coefficient R^2 being equal to 94.65%. It was determined that feed and the corresponding interactions contributed more than 45% to the model's R^2 , followed by the depth of cut and the machining condition. In addition, the cutting speed was the variable with the least effect on the response. The Non-Dominated Sorting Genetic Algorithm 2 (NSGA-II) was employed to identify the front of optimal solutions that consider both minimizing surface roughness and maximizing Material Removal Rate (MRR). Finally, a set of extra experiments proved the validity of the model by exhibiting relative error values, between the measured and predicted roughness, below 10%.

Keywords: additive manufacturing; CFRP; flooded cooling; machining; NSGA-II; PET-G; regression analysis; surface roughness



Received: 22 December 2024

Revised: 19 January 2025

Accepted: 31 January 2025

Published: 2 February 2025

Citation: Tzotzis, A.; Efkolidis, N.; Cheng, K.; Kyratsis, P. Multiple Regression Analysis and Non-Dominated Sorting Genetic Algorithm II Optimization of Machining Carbon-Fiber-Reinforced Polyethylene Terephthalate Glycol Parts Fabricated via Additive Manufacturing Under Dry and Lubricated Conditions. *Lubricants* **2025**, *13*, 63. <https://doi.org/10.3390/lubricants13020063>

Copyright: © 2025 by the authors. Licensee MDPI, Basel, Switzerland. This article is an open access article distributed under the terms and conditions of the Creative Commons Attribution (CC BY) license (<https://creativecommons.org/licenses/by/4.0/>).

1. Introduction

Surface quality during machining is a critical factor influencing the performance, esthetics, and functionality of machined components. It encompasses parameters such as surface roughness, waviness, and geometric accuracy, which collectively determine the texture and precision of the finished surface. The average surface roughness, often denoted as R_a , is particularly significant as it directly impacts fatigue resistance, wear resistance, friction, and even the adhesion properties of coatings. Achieving an optimal surface finish is essential in manufacturing industries that deal with components related to vehicles, structures, and devices, where high-precision components are required. The machining process variables, such as cutting speed, feed rate, depth of cut, and tool geometry, play a vital role in determining surface quality. Additionally, factors like material properties, tool wear, and machine vibrations can introduce variations, making it a complex area of study.

Several investigations on the surface roughness are available in the bibliography, as well as evaluations of the surface quality of a wide variety of materials, including Aluminum Alloys (AAs) such as 6061 [1,2] and 6063 [3], steels such as EN36 alloy steel [4], 316L stainless steel [5], and SS410 steel [6], as well as superalloys such as Nimonic C263 [7] and Inconel 600 [8]. The technological advancements in material science, and especially the advent of composite materials, dictated a new direction in surface quality evolution. Kannan et al. [9] investigated the surface roughness, tool wear, and cutting forces induced during the turning of AA7075/SiC/Gr hybrid composite by utilizing the Taguchi method. Similarly, Bhushan [10] worked on the impact that tool tip radius and typical machining parameters have on the generated surface quality of the AA7075/Si composite. The author employed the design of experiments and experimental work to assess the aforementioned parameters. Shanmugavel et al. [11] presented a work on the Al-Mg-MoS₂ reinforced composite Wire Electrical Discharge Machining (WEDM). The authors examined a variety of machining parameters on the produced surface quality. Besides the metal matrix composites, the scientific community shows an increasing interest in another composite material group, namely the fiber-reinforced polymers. John et al. [12] investigated the machining parameters influence on the surface quality of Polypropylene (PP), reinforced with natural fibers. The authors focused on the milling process and the reinforcement with jute and rice husk fibers. In a similar manner, Ravikumar et al. [13] presented research on the jute/polyester composite drilling, evaluating the delamination and the surface roughness during the process. The surfaces of the used specimens were treated with sodium bicarbonate solution. Altin Karataş et al. [14] worked on the abrasive waterjet drilling of Carbon-Fiber-Reinforced Polymer (CFRP) with respect to the fiber orientation angles. The surface roughness and the delamination factor were the output parameters studied by the authors. Slamani et al. [15] used carbide end-mills to process the flax fiber reinforced polymer, with epoxy resin matrix, for evaluating the slot milling parameters on the generated surfaces.

In general, both metal matrix composites and fiber-reinforced composites constitute two material groups that are widely used in the industry. Especially the CFRP composites have been widely studied due to their superior mechanical properties, in combination with their light weight. In addition, the advent of additive manufacturing enabled the production of specialized components made of CFRP filaments, which are commonly used by industries such as aerospace and automotive. The fabricated components usually require post-processing to acquire their final shape and dimensions, improving their functionality. Despite the fact that AM is a relatively new technology, an increasing number of studies are available for the post-processing of 3D-printed standardized polymers such as the abrasive flow machining of Acryl Butadiene Styrene (ABS) and Polylactic Acid (PLA) [16], laser cutting of ABS [17], acetone vapor jet drilling of ABS [18], and ultrasonic drilling of PLA [19]. However, the number of studies related to the post-processing of composite filaments, and especially CFRP, is still limited, with the machining processes focusing mostly on either milling or orthogonal cutting. Gómez-García et al. [20] investigated the machinability aspects of the 3D-printed Polyether Ether Ketone (PEEK), reinforced with short carbon fibers composite, during orthogonal cutting. Hassan et al. [21] utilized the Finite Element Method (FEM) to simulate and evaluate the milling process of 3D-printed CFRP parts. Guo et al. [22] worked on the carbon-fiber-reinforced PEEK dry milling by analyzing the machining behavior of additively manufactured parts of different raster angles. Wei et al. [23] investigated the efficiency of the hole-making techniques with the milling operation. The authors worked with 3D-printed, fiber-reinforced plastic components. Similar studies focus on the 3D-printed CFRP material during face milling under dry conditions [24], during slot milling under both dry and cooling conditions [25],

as well as during dry milling with coated carbide tools [26]. Besides machining post-processing, neosanding [27] and ironing [28] are equivalent methods used to post-process the raw 3D-printed surfaces of parts for increased surface smoothness and quality.

Parallel to surface quality, the Material Removal Rate (MRR) is a key performance metric in machining. MRR refers to the volume of material removed per unit of time and directly influences productivity and cost-effectiveness. A higher MRR enables faster manufacturing, reducing lead times and operational costs, which is crucial in mass production [29–31]. However, achieving high MRR often conflicts with maintaining superior surface quality, as aggressive cutting parameters can lead to increased surface roughness and defects such as chatter marks or thermal damage. Balancing these conflicting objectives requires a comprehensive understanding of machining dynamics and the optimization of process parameters. The interplay between surface quality and MRR underscores the importance of modern manufacturing technologies, including advanced tooling, process monitoring, and data-driven optimization. By addressing these challenges, manufacturers can achieve efficient production without compromising the functional integrity of the components, contributing to sustainable and competitive industrial practices.

The literature survey revealed that a limited number of studies deal with the machining of additively manufactured materials, and especially composites. In addition, a research gap related to the post-processing turning of 3D-printed CFRP materials under lubricated conditions has been identified. In light of the above, the present study investigates the influence of the standard machining conditions, such as cutting speed, feed rate, and depth of cut during turning, on the surface quality of the additively manufactured Polyethylene Terephthalate Glycol (PET-G)-based CFRP, under both dry and lubricated conditions. The interaction of the coolant with the machined surface is of particular interest in the specific material group due to the lack of specialized coolants and systems. To assess the influence of the aforementioned parameters, a regression analysis was performed, and the Non-Dominated Sorting Genetic Algorithm 2 (NSGA-II) was used to identify the optimal cutting parameters for achieving a compromise between acceptable surface finish and rapid cutting operations.

2. Materials and Methods

The present study deals with the experimental investigation of the 3D-printed PET-G-based CFRP during the turning process. It is divided into four steps as shown in Figure 1.

First, the experiments were designed according to the selected conditions, leading to 54 experiments (27 experiments for dry conditions and 27 experiments for lubricated conditions, respectively). In addition, the equivalent workpieces were fabricated. Next, the CNC machine was set, and the cutting experiments were carried out with the BOXFORD 160TCL CNC lathe. During the third step, the surface roughness and the equivalent profiles were measured with the DIAVITE DH-8 gauge. Finally, the collected data were organized, and the regression analysis was realized.

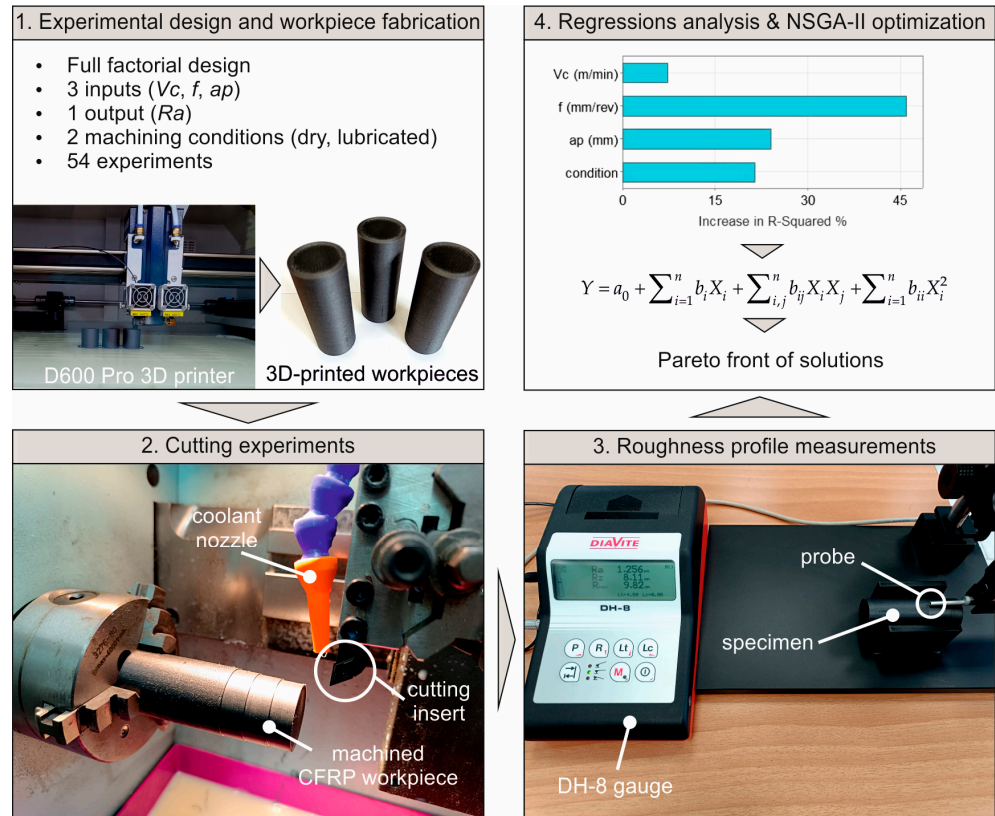


Figure 1. The experimental setup and workflow of this study.

2.1. Experimental Settings and Testing Materials

The selected material comprises 80 wt% PET-G and 20 wt% carbon fiber. It is known for its increased stiffness and durability, as well as for the resistance in higher temperatures. The previously mentioned advantages make it ideal for the manufacturing of shells intended to be used in unmanned vehicles. Table 1 contains the basic properties of the filament. It should be noted that according to the manufacturer, Yield strength σ_y , Yield strain ϵ_y and Strain at break ϵ_b were tested at 50 mm/min speed, whereas the Young’s modulus E at 1 mm/min.

Table 1. Basic properties of the used CFRP filament [32].

Property	Value
Density, ρ	1.19 g/cm ³
Young’s modulus, E	3.8 GPa
Yield strength, σ_y	52.5 MPa
Yield strain, ϵ_y	4.2%
Strain at break, ϵ_b	8%
Heat deflection temperature, T_d	80 °C

Table 2 presents the settings used to fabricate the specimens with the CreatBot D600 Pro printer by utilizing the Fused Deposition Modeling (FDM) method. A nozzle with a 0.6 mm diameter was utilized, and filaments of 1.75 mm size. All settings were set according to the suggestions provided by the manufacturer (NEEMA3D™) [32] through personal communication. The specific shell thickness, the infill density, and the infill pattern were selected with the depth of cut in mind. Moreover, the rigidity of the workpieces was also taken into account.

Table 2. The settings for the additively manufactured workpieces.

Setting	Value
Nozzle temperature	255 °C
Bed temperature	70 °C
Layer thickness	0.2 mm
Printing speed	40 mm/s
Flow rate	1.0
Shell thickness	3 mm
Infill density	50%
Infill pattern	Rectilinear

Table 3 presents the selected cutting conditions: cutting speed (V_c), feed (f), and depth of cut (ap), as well as the boundaries of their values. In addition, Table 3 indicates that this study was performed under both dry and lubricated conditions. The selection of the range of the cutting conditions was based on the recommendations of the tool manufacturer for light to finishing operations, in addition to the study by Venkatesh et al. for pure PET-G [33]. The used cutting inserts and the tool holder have designation numbers DCGT090202N-SC and SDJCL1010-03S, respectively. Additionally, the lubricated cuts were performed with the flooded cooling method by applying the Refan 150 mineral coolant, mixed with water at proportions of 5–95%.

Table 3. The predictors of the regression analysis.

	Continuous Predictors			Categorical Predictor
	V_c (m/min)	f (mm/rev)	ap (mm)	Condition
Upper boundary	285	0.11	2.0	1 (lubricated)
Lower boundary	115	0.05	0.5	0 (dry)

2.2. Design of Experiments and Measured Responses

The experiments were designed according to the full factorial design for acquiring a dense dataset. Table 4 shows the measured surface roughness arithmetic mean for both dry ($Ra,0$) and lubricated ($Ra,1$) conditions. In addition, Table 4 includes the calculated MRR for each one of the condition combinations, which were used in Section 3.2 for determining the optimal solutions that minimize the generated surface roughness on the one hand and maximize the MRR on the other. To calculate the MRR, Equation (1) was used.

$$MRR(\text{cm}^3/\text{min}) = V_c \times f \times ap \quad (1)$$

The comparison between the experimental measurements of the dry and the lubricated experiments revealed that the summation of the lubricated cuts exhibited improved surface quality compared to the dry ones. Figure 2 illustrates this comparison, highlighting that the improvement in surface quality is significant for the majority of the experiments, with the exception of experiment number 24. In addition, it is shown that the average decrease in surface roughness for the three cutting speed levels: 115 m/min, 200 m/min, and 285 m/min, is approximately 20.7%, 21.6%, and 26.1%, respectively. The results during dry conditions testing are of similar magnitude to the ones reported by Alzyod et al. [27] for neosanding of PLA and subtractive processing [34] of ABS. In addition, the work of Juneja et al. [18] on ABS acetone vapor processing presented findings related to the surface roughness that match the ones of the present study. Cococetta et al. [25] reported reduced burr and better overall surface quality for both edge and slot milling of 3D-printed CFRP

specimens under Minimum Quantity Lubrication (MQL) conditions. A more thorough discussion on the influence of the parameters on the generated roughness is made in Section 3. Despite the fact that the non-machining post-processing methods mentioned earlier provide good results in general, the surface finish and dimensional accuracy that the machining methods provide are superior, especially under lubricated conditions. The drawback when utilizing machining is the more complicated setup and the requirement of CNC machines. Specifically, ironing and neosanding can be realized with the 3D printer itself, whereas acetone vapor deposition can be realized with simple equipment of low cost. However, these methods cannot be applied with the same efficiency to all types of 3D-printed materials [35]. Finally, when evaluating the lubricated machining, flooded cooling provides equal results compared to MQL, with a simpler setup.

Table 4. The experiments according to the full factorial design and the corresponding results.

Number	V_c (m/min)	F (mm/rev)	ap (mm)	MRR (cm ³ /min)	$Ra,0$ (μ m)	$Ra,1$ (μ m)
1	115	0.05	0.50	2.88	1.823	1.402
2	115	0.05	1.25	7.19	2.198	1.960
3	115	0.05	2.00	11.50	2.301	1.874
4	115	0.08	0.50	4.60	2.009	1.568
5	115	0.08	1.25	11.50	2.580	2.065
6	115	0.08	2.00	18.40	2.308	2.001
7	115	0.11	0.50	6.33	2.566	1.899
8	115	0.11	1.25	15.81	3.090	2.790
9	115	0.11	2.00	25.30	3.362	2.863
10	200	0.05	0.50	5.00	1.762	1.455
11	200	0.05	1.25	12.50	1.989	1.949
12	200	0.05	2.00	20.00	2.253	1.878
13	200	0.08	0.50	8.00	2.020	1.512
14	200	0.08	1.25	20.00	2.744	2.041
15	200	0.08	2.00	32.00	2.466	2.089
16	200	0.11	0.50	11.00	2.788	1.893
17	200	0.11	1.25	27.50	3.067	2.700
18	200	0.11	2.00	44.00	3.255	2.865
19	285	0.05	0.50	7.13	2.121	1.562
20	285	0.05	1.25	17.81	2.262	2.102
21	285	0.05	2.00	28.50	2.453	2.247
22	285	0.08	0.50	11.40	2.429	1.788
23	285	0.08	1.25	28.50	3.288	2.541
24	285	0.08	2.00	45.60	2.616	2.510
25	285	0.11	0.50	15.68	3.199	1.975
26	285	0.11	1.25	39.19	3.566	2.856
27	285	0.11	2.00	62.70	3.890	2.905

To assess whether the surface roughness measurements follow a normal probability distribution, the probability plot of Figure 3 was plotted, according to the Anderson–Darling test, with the confidence level set to 95%. It is evident that the data points (blue dots) mostly align well with the straight line representing the distribution, indicating that the Ra values follow the normal distribution reasonably well. There may be minor deviations at the tails (extreme low and high Ra values). However, it is shown that these two points do not fall significantly outside the confidence bands (curved lines). Finally, the points' tight clustering around the distribution line suggests that the Ra measurements have a consistent variance, supporting the validity of the normality assumption.

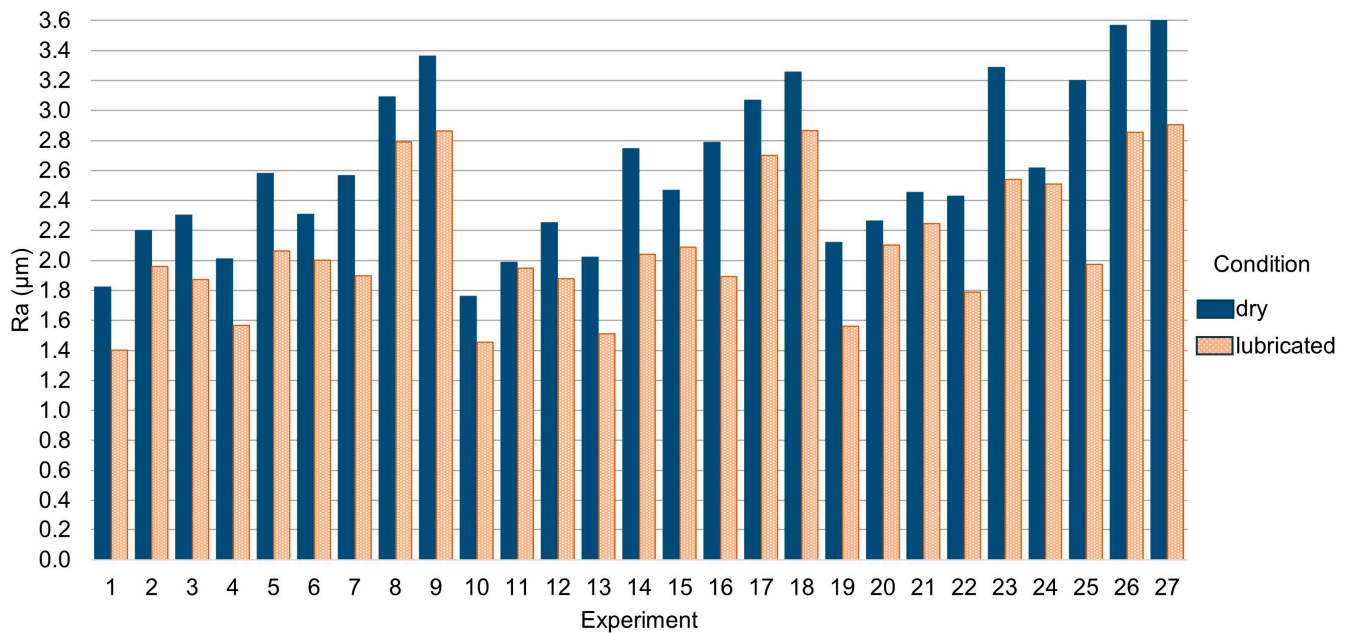


Figure 2. Comparison between the measured surface roughness under dry and lubricated conditions.

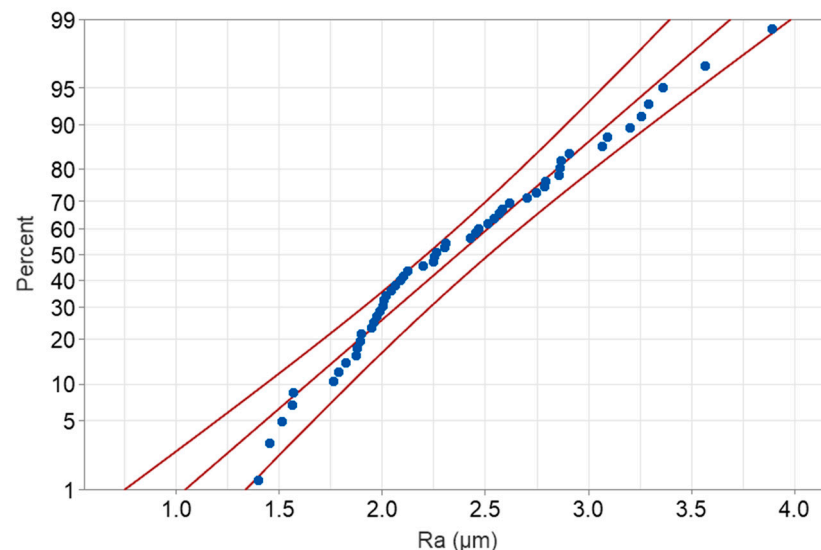


Figure 3. Probability plot of the experimental surface roughness values.

2.3. Multiple Regression Analysis

Multiple regression analysis is a statistical method used to model the relationship between a dependent variable and multiple independent variables. It predicts the dependent variable by fitting a linear equation that minimizes the difference between observed and predicted values. In machining studies [36–38], it helps identify how factors like cutting speed, feed rate, and depth of cut influence surface roughness. The method can include interaction terms to capture combined effects of variables.

Equations (2) and (3) represent the regression model derived from the analysis of the experiential data. Specifically, Equation (2) can be used to predict the surface roughness of the process under dry conditions, whereas Equation (3) is for the surface roughness prediction under lubricated conditions. Both mathematical representations are expressed by considering the predictors and their cross-term interactions, as well as the quadratic terms. The regression analysis was carried out by employing the backward elimination [39] for simplifying the derived model.

$$Ra,0(\mu\text{m}) = 1.933 - 0.00614V_c - 16.16f + 1.217ap + 0.000021V_c^2 + 184.3f^2 - 0.4775ap^2 + 3.59f \times ap \quad (2)$$

$$Ra,1(\mu\text{m}) = 1.951 - 0.00713V_c - 22.28f + 1.364ap + 0.000021V_c^2 + 184.3f^2 - 0.4775ap^2 + 3.59f \times ap \quad (3)$$

To determine the statistical significance of the terms and evaluate their contribution, the analysis of variance (ANOVA) of the response data was performed. Table 5 shows the ANOVA results in terms of the mean square values, the f -value, and the p -value. The goodness of fit, the variance, and the prediction capabilities were analyzed by setting a 95% confidence level. The coefficients R^2 , R^2 (adjusted), and R^2 (predicted) were calculated equal to 94.65%, 93.24%, and 91.26%, respectively, indicating a strong fit and adequate prediction accuracy due to the increased variability explained. To assess the statistical significance of the model, the p -values were used. Therefore, each term with a p -value lower than $\alpha = 0.05$ is considered statistically significant. However, this does not imply that all statistically significant terms influence the response to a considerable degree. The contribution was evaluated with the f -value of each term, which is described as the ratio of the mean square to the error mean square. It was found that the three continuous predictors and the categorical term are responsible for influencing the response by 87%.

Table 5. Analysis of variance results for the multiple regression model.

Source	Degrees of Freedom	Sum of Squares	Mean Square	f -Value	p -Value	Contribution %
Model	11	16.2236	1.47487	67.49	0.000	
Error	42	0.9178	0.02185			
Total	53	17.1414				
R-sq = 94.65%, R-sq (adj) = 93.24%, R-sq (pred) = 91.26%						
Term						
V_c	1	0.8867	0.8867	40.58	0.000	5.47
f	1	7.0561	7.0561	322.89	0.000	43.49
ap	1	2.9843	2.9843	136.56	0.000	18.39
condition	1	3.1848	3.1848	145.74	0.000	19.63
V_c^2	1	0.2816	0.2816	12.88	0.001	1.73
f^2	1	0.3302	0.3302	15.11	0.000	2.04
ap^2	1	0.8656	0.8656	39.61	0.000	5.34
$V_c \times \text{condition}$	1	0.0643	0.0643	2.94	0.094	0.40
$f \times ap$	1	0.1567	0.1567	7.17	0.011	0.97
$f \times \text{condition}$	1	0.3032	0.3032	13.88	0.001	1.87
$ap \times \text{condition}$	1	0.1101	0.1101	5.04	0.030	0.68

The contribution of each one of the independent variables is shown in Figure 4. It is evident that feed has the largest impact on the model, contributing approximately 45% to the coefficient of determination R^2 increase. This finding aligns with the fact that feed rate is typically the most significant factor influencing surface roughness, as it directly determines the spacing between tool marks. Depth of cut contributes the second most to the model, with a noticeable but smaller effect than feed. This is expected because deeper cuts increase cutting forces, vibrations, and tool deflection, thereby affecting roughness. The condition adds a moderate amount to the explained variance. This indicates that lubrication plays an important role in controlling friction, heat dissipation, and chip evacuation, all of which can influence surface finish. Finally, cutting speed contributes the least to the model, suggesting that its effect on surface roughness is relatively minor compared to the other variables. The reason for this is probably the fact that cutting speed affects surface roughness indirectly, as it modifies the thermal and dynamic effects and does not directly relate to the geometrical aspects of the process. To further visualize the order of variables' contributions, the Pareto graph from Figure 5 was added.

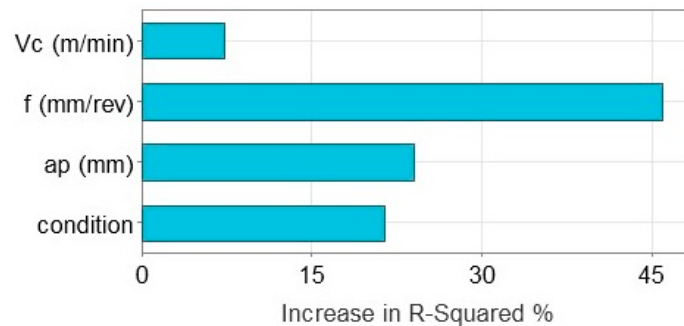


Figure 4. Incremental impact of the variables for the contribution of new information to the model.

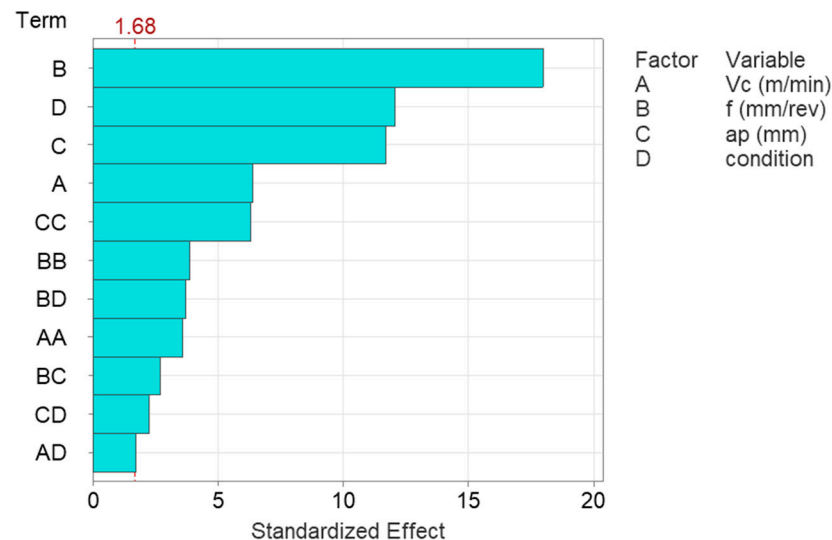


Figure 5. Pareto graph for the contribution of the variables and their interactions.

In summary, feed rate dominates, as it has the most significant impact on surface roughness, likely due to its direct relationship with tool mark spacing. Depth of cut and lubrication conditions provide additional explanatory power, likely through their influence on cutting forces and material behavior, whereas cutting speed is less influential, likely because its effects are secondary compared to the geometric and force-driven variables.

3. Results and Discussion

3.1. Analysis of Predictors' Behaviors on the Generated Surface Roughness

The mean effect plot of Figure 6 provides detailed insights into how the four variables influence surface roughness in additively manufactured CFRP turning. It is evident that the produced surface roughness in dry conditions is noticeably higher ($\sim 2.6 \mu\text{m}$), indicating rougher surfaces when no lubrication is used. On the contrary, lubricated conditions reduce roughness significantly ($\sim 2.1 \mu\text{m}$), suggesting that lubrication improves the surface finish by reducing friction and thermal effects. Cutting speed exhibits a more complex pattern. At low speed (115 m/min), R_a values start close to $2.25 \mu\text{m}$, showing acceptable levels of roughness. Medium speed (200 m/min) does not seem to affect R_a , showing no significant change. On the contrary, cutting speed beyond 200 m/min increases R_a significantly ($\sim 2.7 \mu\text{m}$), indicating poorer surface quality, possibly due to thermal effects and material degradation at high speeds. Lower feeds are responsible for the production of low R_a values ($< 2.0 \mu\text{m}$), reflecting smoother surfaces. Medium feeds increase roughness moderately ($\sim 2.4 \mu\text{m}$), whereas at the highest feed (0.11 mm/rev), R_a peaks ($\sim 2.9 \mu\text{m}$), indicating significantly rougher surfaces due to higher material removal rates and tool vibrations. Therefore, it is obvious that feed rate has the most pronounced effect, with

roughness increasing sharply as feed increases. This effect was expected as it is standard for a wide variety of materials such as CFRPs [25], aluminum [40], and Ti6Al4V [41]. Moreover, a similar pattern for feed rate was identified in a previous work of the authors [42] for the same material. Finally, it is observed that depth of cut acts increasingly when shifting from low to medium depths. Specifically, the lowest depth (0.50 mm) yields Ra values below $2.0 \mu\text{m}$, indicating a smoother finish. At medium depth (1.25 mm), Ra increases sharply at $\sim 2.55 \mu\text{m}$, reflecting a rapid deterioration in surface finish due to increased cutting forces and tool interaction. In contrast, beyond this point, Ra continues to increase slightly ($\sim 2 \mu\text{m}$). The sudden increase in Ra when shifting depth of cut from lower to higher values, followed by a recession when further increasing depth of cut was reported by El Mehtedi et al. [43] for the PET-G milling. Additionally, Abena et al. [44] correlated the deeper cuts with the surface deterioration for the orthogonal cutting of CFRP.

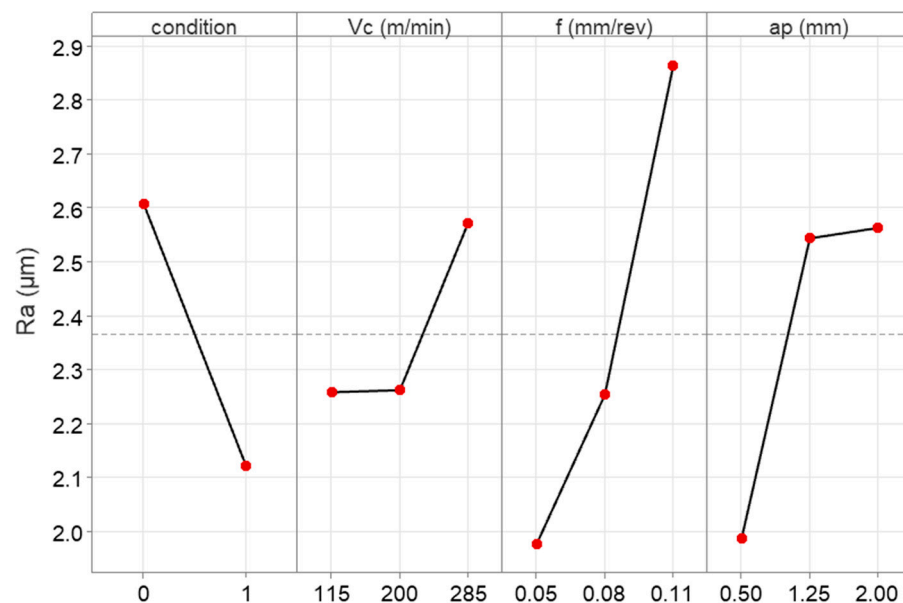


Figure 6. The main effect plots for the experimental surface roughness with respect to the condition, cutting speed, feed, and depth of cut.

In summary, feed is the most critical variable, causing a sharp rise in Ra at higher levels. Lubrication significantly reduces roughness, making it essential for improving surface finish. Low depths of cuts produce a smooth surface, but a sharp increase occurs at the medium level, with no further effect at the high level. Low and medium speeds produce acceptable levels of Ra , while high speeds degrade the surface considerably. In addition, the analysis highlights that controlling feed and depth of cut at low levels, combined with lubrication, is key to achieving optimal surface quality during CFRP turning.

The contour plots of Figure 7 illustrate the interaction effects between the cutting parameters on the surface roughness during turning under dry conditions. The color gradient represents ranges of Ra , where blue shades correspond to smoother surfaces and green shades indicate rougher surfaces. Figure 7a illustrates the interaction between feed and speed. It is observed that surface roughness remains low ($Ra < 2.5 \mu\text{m}$) at low feed rates ($f < 0.072 \text{ mm/rev}$) irrespective of V_c . Higher feed rates ($f > 0.08 \text{ mm/rev}$) increase Ra significantly, especially as V_c approaches higher levels (280 m/min). This is due to the dominant influence of feed on the surface geometry. At low feed, V_c has a marginal effect on Ra , while at high feed, Ra increases notably at higher V_c values). Figure 7b describes the interaction between depth of cut and speed. Lower depths of cuts contribute towards lower surface roughness values, even as V_c increases, indicating minimal influence of cutting speed at small depths. There is a noticeable rise in Ra at higher speeds, for both medium

and high levels of ap . However, the pattern beyond $ap = 1.5$ mm suggests that extreme depths of cut do not significantly affect Ra further. The interaction between depth of cut and feed (Figure 7c) revealed that at low feed ($f < 0.072$ mm/rev), surface roughness remains low across all depth values, indicating a smooth finish at these settings. On the contrary, at high feed ($f > 0.096$ mm/rev), Ra increases drastically, especially for larger depths, as both feed and depth of cut strongly influence surface roughness through chip formation and material deformation.

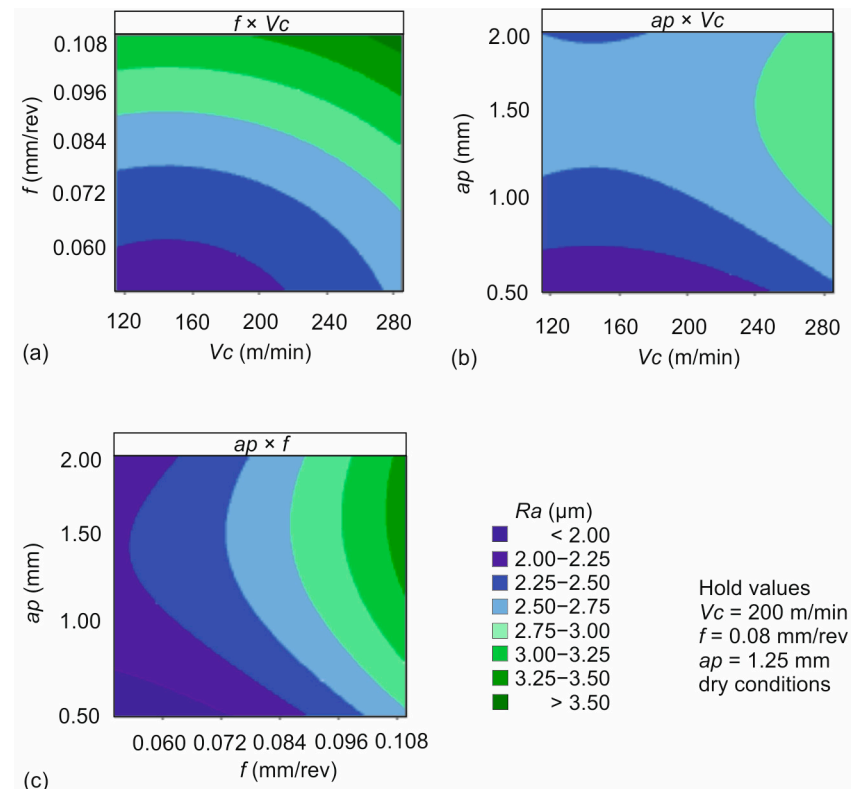


Figure 7. The contour plots of the surface roughness, based on the regression model for the dry conditions: (a) $f \times V_c$, (b) $ap \times V_c$, and (c) $ap \times f$.

Summarizing, these plots emphasize that surface roughness is highly dependent on the interaction between the parameters, with feed being the most critical factor. Cutting speed primarily influences Ra in combination with high feed or depth of cut but has a minor effect at low levels of feed and depth of cut. Finally, depth of cut significantly affects Ra , only when combined with high feed rates.

Similarly, Figure 8 illustrates the interaction effects of cutting speed, feed, and depth of cut on the surface roughness under lubricated conditions. The color gradient indicates Ra , with blue representing smoother surfaces ($Ra < 1.75 \mu\text{m}$) and green indicating rougher surfaces ($Ra > 2.75 \mu\text{m}$). Figure 8a shows the interaction between feed and speed. At low feeds, surface roughness is minimal ($Ra < 2.0 \mu\text{m}$) across all speed values, highlighting the benefits of lubrication in achieving a smoother finish. Ra increases significantly at higher feeds, particularly at higher speed values (above 240 m/min). The combined effect of increased f and V_c causes a rougher finish. In addition, higher cutting speeds mitigate roughness at lower feeds, but at high feeds, the influence of speed becomes less significant. The interaction between depth of cut and speed is shown in Figure 8b. Surface roughness remains below $2.0 \mu\text{m}$ across all speed values for lower depths. At medium to high depth of cut values, Ra increases moderately, particularly at high speed values. However, the roughness is less severe compared to dry conditions, showing that lubrication reduces the adverse effects of increasing depth of cut. In general, lower depths and speed provide

smoother surfaces. Finally, Figure 8c illustrates the interaction between depth of cut and feed. At low feed rates, surface roughness remains minimal ($Ra < 1.75 \mu\text{m}$) across all ap values. At high feed rates, as expected, Ra increases sharply, particularly at depths above 1.5 mm. This shows that even with lubrication, high f and ap contribute significantly to roughness. Moreover, even though roughness increases with increasing ap , lubrication helps control the extent of this rise.

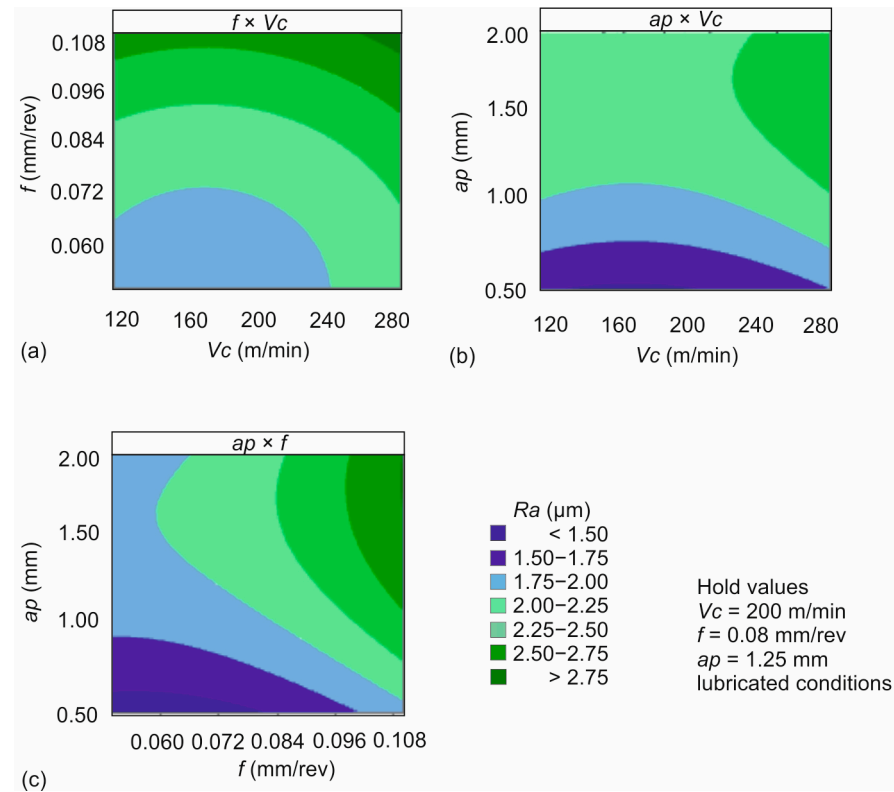


Figure 8. The contour plots of the surface roughness, based on the regression model for the lubricated conditions: (a) $f \times V_c$, (b) $ap \times V_c$, and (c) $ap \times f$.

Summarizing, it is evident that lubrication significantly reduces Ra compared to dry conditions, particularly at low feed and depth-of-cut levels. Feed remains the most influential factor, as higher feed rates consistently increase Ra , regardless of lubrication. Cutting speed has a minor effect at low feed and depth of cut, but it interacts more strongly at high levels of these parameters. Finally, depth of cut has a moderate influence, with higher values leading to rougher surfaces, but lubrication reduces its overall impact. These results emphasize the importance of lubrication in minimizing surface roughness, especially at lower feed rates and depths of cut.

Figures 9 and 10 constitute a graphical representation used to visualize the relationships between the three variables in the dataset, supplementing the contour plots. Moreover, these plots visualize the solutions of Equations (2) and (3) respectively, within the studied range of cutting conditions. Specifically, Figure 9 illustrates this relationship for the dry conditions, whereas Figure 10 is for the lubricated conditions. Summarizing, it is shown that higher cutting speeds contribute towards higher surface roughness values. Increased feed rates consistently result in higher surface roughness, making it the most influential parameter for Ra . While depth of cut exhibits a strong effect, its impact is less significant than feed rate in determining surface roughness, with lower values of depth of cut contributing towards better surface quality. Finally, it is evident that above a certain depth, surface roughness is no longer influenced.

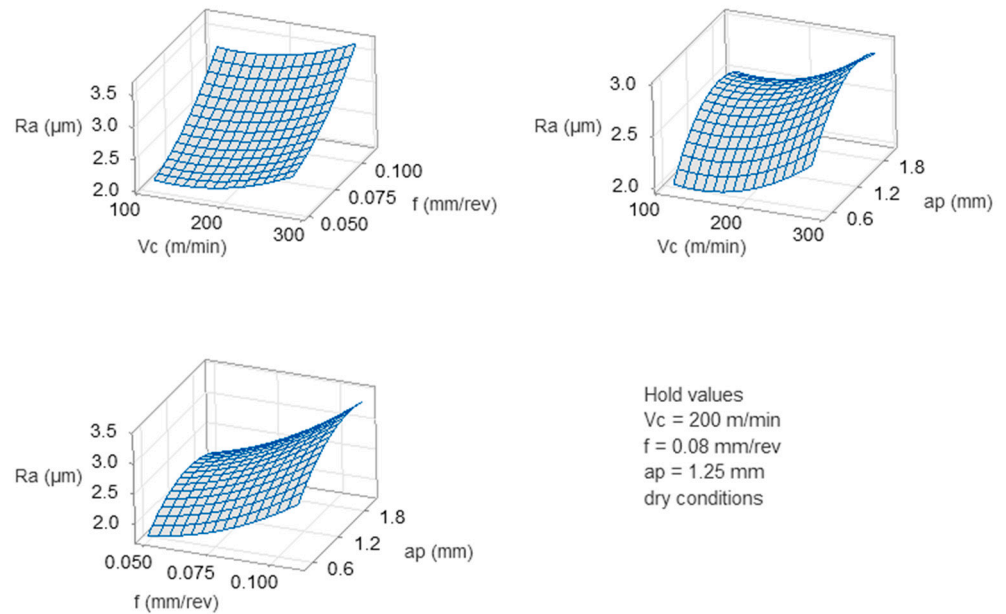


Figure 9. The 3D surface plots for the dry conditions.

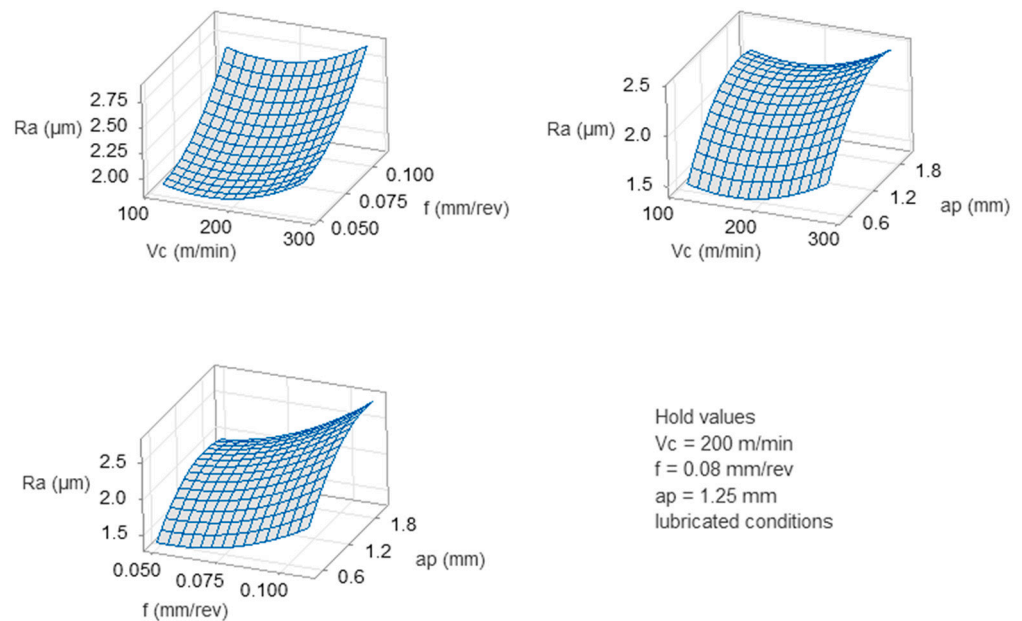


Figure 10. The 3D surface plots for the lubricated conditions.

3.2. Optimization of the Cutting Conditions by Utilizing the NSGA-II Algorithm

To optimize the process, both MRR and R_a were taken into account because during light and finishing, the final production cost is a compromise between quality and time. For this purpose, the NSGA-II algorithm was employed. It is a popular multi-objective optimization algorithm, widely used for solving problems with conflicting objectives [45,46]. It employs a population-based approach to identify a set of Pareto-optimal solutions in a single run. NSGA-II ranks solutions using non-dominated sorting and maintains diversity through a crowding distance mechanism. It combines crossover and mutation operators for exploration and refinement of solutions. Fast sorting, elitism (retaining the best solutions), and reduced computational complexity make it efficient and scalable. For the problem stated in this study with the three continuous variables, the population was set to 200, the maximum number of generations to 50, and no stopping criteria were set. Figure 11 depicts the optimization process. In specific, Figure 11a,b are the Pareto fronts of solutions for the

dry and lubricated experiments accordingly. Similarly, Figure 11c,d illustrate the variable combinations that generated the solutions.

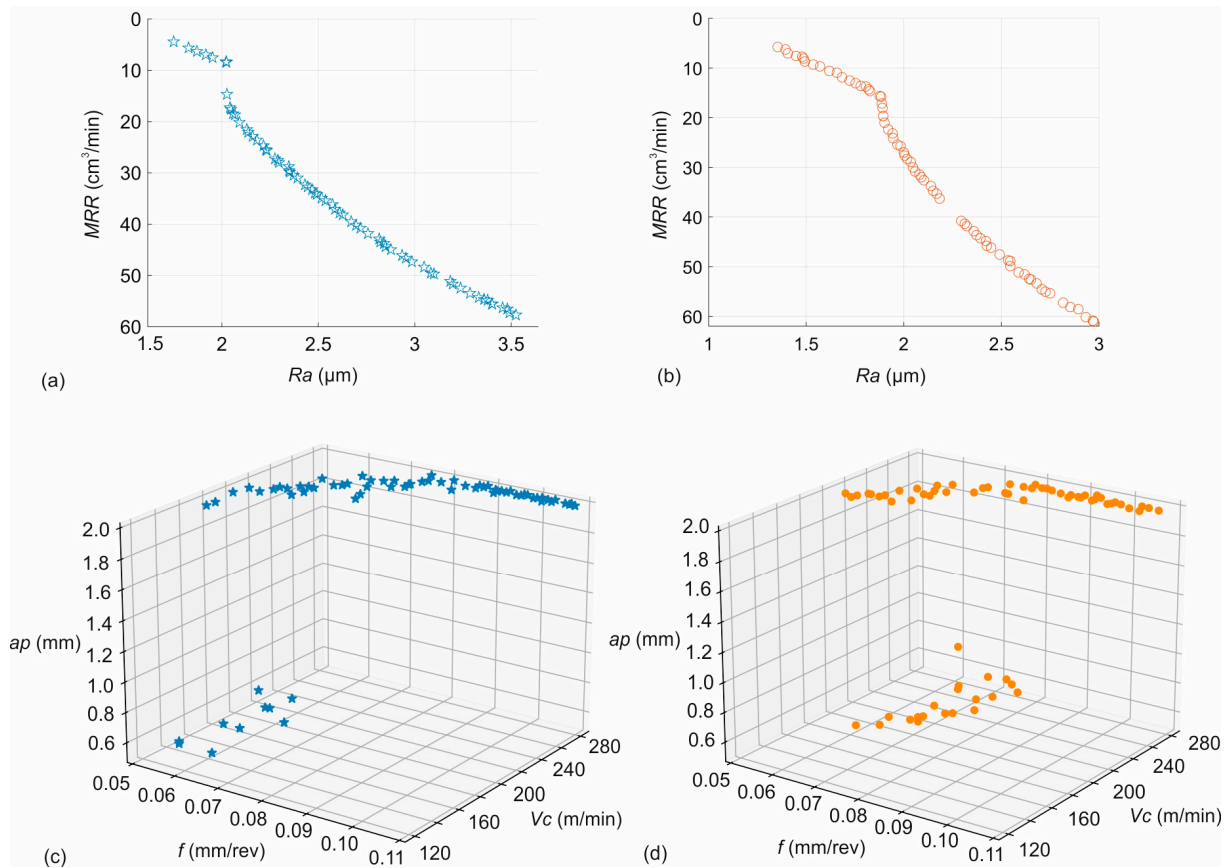


Figure 11. The optimization plots: (a) Pareto front for the dry conditions, (b) Pareto front for the lubricated conditions, (c) the corresponding solutions for the dry conditions, and (d) the corresponding solutions for the lubricated conditions.

3.3. Performance Validation of the Regression Model

The scatter plots of Figure 12 were used to compare the experimental surface roughness values measured during the experiments and the predicted values, calculated by the regression model for the two conditions: dry and lubricated. By observing Figure 12a for the dry conditions, the red line represents the ideal relationship, where the predicted and experimental values perfectly match. The scatter points closely align with the red line, indicating that the regression model performs well under dry conditions. Slight deviations at higher Ra values (between $3.0\ \mu\text{m}$ and $3.5\ \mu\text{m}$) suggest that the model may slightly underpredict or overpredict surface roughness for extreme cases. Figure 12b shows that the scatter points are closer to the fit line compared to Figure 12a, indicating that the regression model is more accurate under lubricated conditions. Deviations appear smaller overall, suggesting that lubrication conditions reduce variability and improve predictability.

In summary, both plots demonstrate a strong correlation between experimental and predicted Ra , showing the regression model's capability to capture key trends in surface roughness. The tighter clustering of points around the fit line in Figure 12b suggests that the model is more reliable when lubrication is used, likely because the process is less influenced by uncontrolled factors like heat or friction.

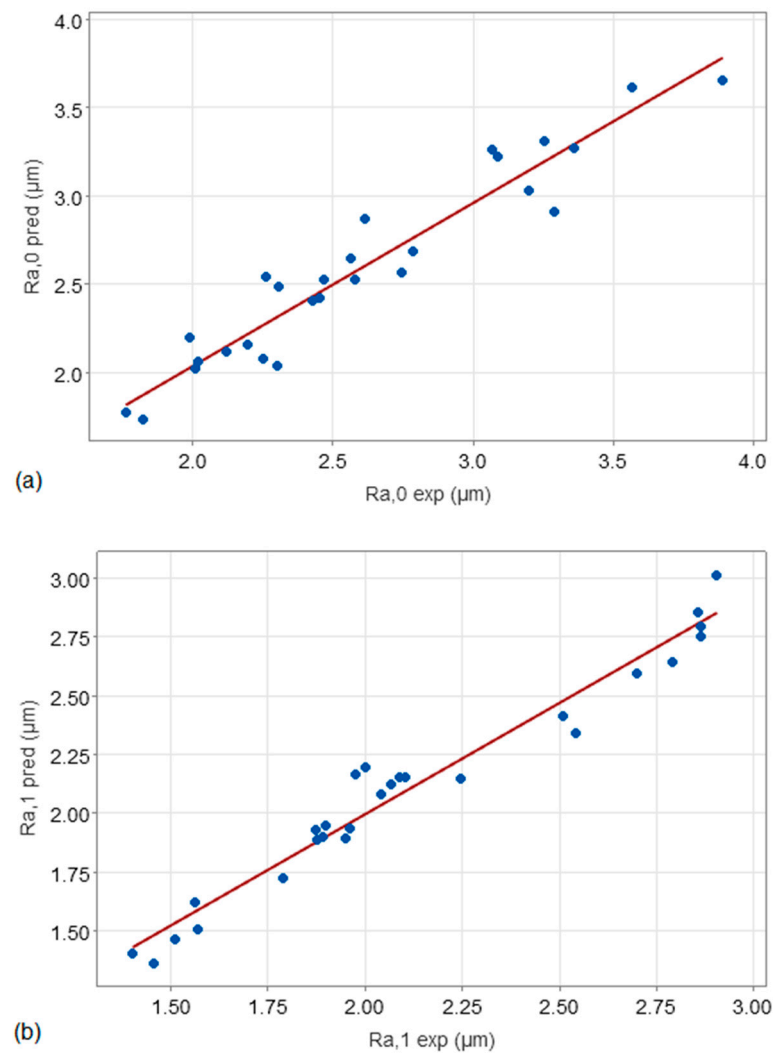


Figure 12. Scatter plots for the comparison between the experimental and the predicted surface roughness values: (a) for the dry conditions and (b) for the lubricated conditions.

A set of validation experiments was performed to assess the prediction capabilities of the model within the range of the selected cutting conditions. The six experiments are shown in Table 6, along with the measured surface roughness and the equivalent predicted values. The computed relative error being below 10% suggests that the model can sufficiently predict the surface roughness under various conditions, within the limits of this study.

Figure 13 depicts sample surface profiles at $V_c = 115$ m/min, $f = 0.05$ mm/rev, and $a_p = 0.50$ mm, and the corresponding roughness measurements for the unmachined material (Figure 13a), as well as the machined surface under both dry (Figure 13b) and lubricated (Figure 13c) conditions. By observing Figure 10, the considerable improvement in quality is noted when considering the change between the unmachined and the machined surfaces. The most noticeable change is the drop in the Ra value, from 15.1 μm to 1.60 μm and 1.00 μm for the dry and lubricated surfaces, respectively. Similarly, the improvement is noticeable in the other surface profile parameters, such as the average maximum profile height Rz , the total profile height Rt , and the maximum profile height R_{max} . The finding that the use of coolant contributes towards reducing Ra and significantly improving the surface quality is supported by the measurements and the macro images. In addition, it is noted that measurements such as R_{max} are greatly reduced with the use of coolant, further supporting the importance of the lubrication conditions during 3D-printed CFRP machining. Even

between dry and lubricated conditions, the reduction is about 78%. This fact is probably based on the abrasive structure of the material [47], as well as on the rougher surfaces that are generally produced by the 3D printing method.

Table 6. Validation experiments and comparison with simulated values.

Test No.	Condition	V_c (m/min)	f (mm/rev)	ap (mm)	$R_{a, exp}$ (μm)	$R_{a, pred}$ (μm)	Relative Error (%)
1	0	125	0.10	0.60	2.595	2.494	4.04
2	0	175	0.08	1.50	2.678	2.570	4.19
3	0	250	0.06	1.20	2.195	2.436	−9.88
4	1	125	0.10	0.60	1.800	1.865	−3.47
5	1	175	0.08	1.50	2.071	2.146	−3.49
6	1	250	0.06	1.20	2.098	2.015	4.10

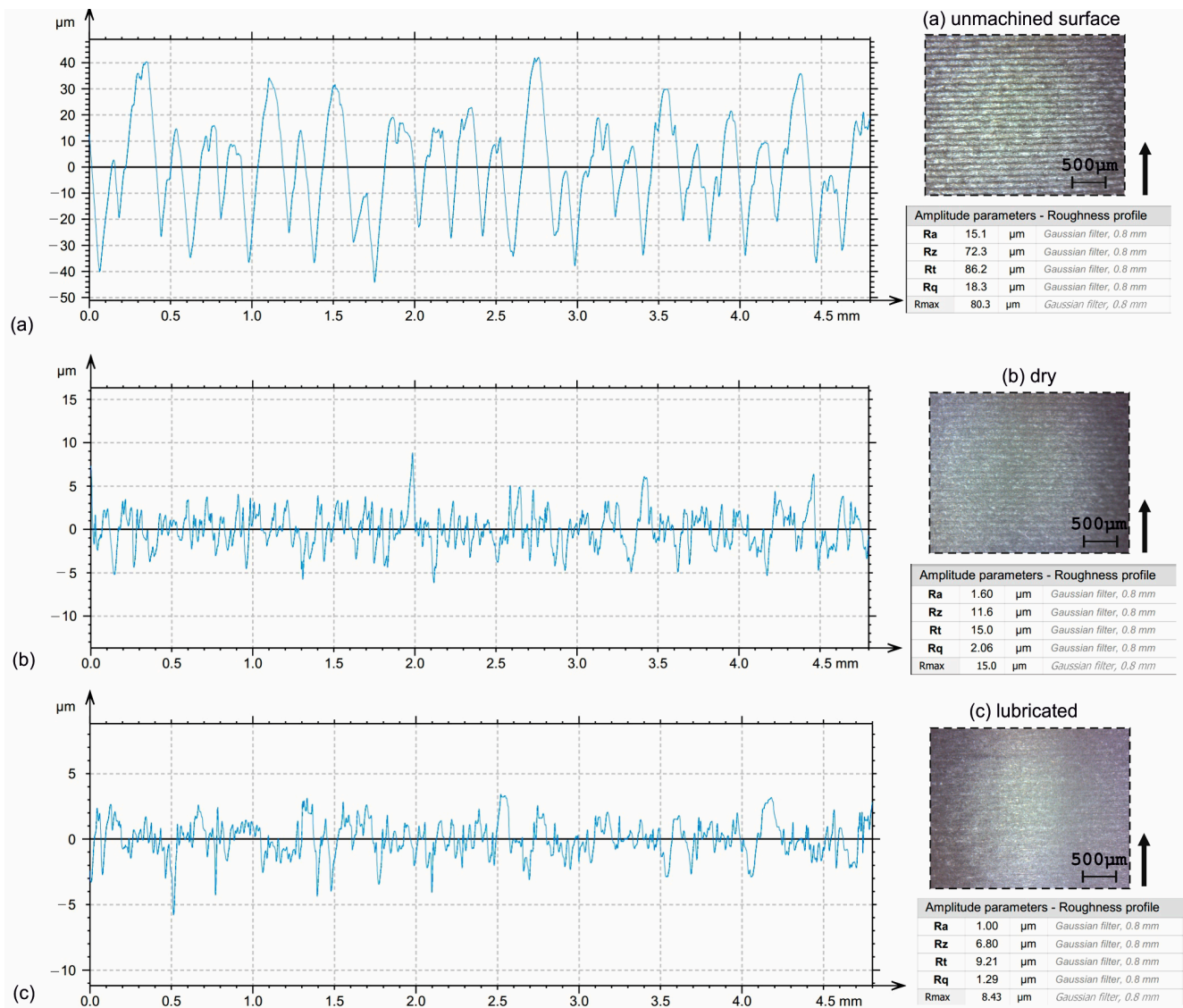


Figure 13. Sample roughness profiles and macro images of: (a) the unmachined surface, (b) dry machined surface, and (c) lubricated machined surface. The arrow indicates the measurement direction.

4. Conclusions

Concluding, this work presents an investigation on the dry and lubricated machining of the 3D-printed PET-G based CFRP. This study includes a regression analysis and an optimization study with the NSGA-II algorithm. The most critical observations derived from this study are as follows:

- The use of coolant acted decreasingly on the generated surface roughness. The average decrease was calculated to be equal to 20.7%, 21.6%, and 26.1% for the three different cutting speed levels, respectively.
- The regression model yielded coefficient values equal to 94.65%, 93.24%, and 91.26% for the R^2 , R^2 (adjusted), and R^2 (predicted) respectively.
- Feed was determined to be the most significant predictor, followed by the depth of cut and the condition. Cutting speed had the least significant effect from the four predictors. However, it cannot be considered negligible.
- The contribution percentages were estimated equal to approximately 46.5%, 24.5%, 22%, and 7% for the feed, the depth of cut, the condition, and the cutting speed, including their interactions, respectively.
- The Pareto fronts of optimal solutions identified combinations that contribute towards minimization of Ra and maximization of MRR. The majority of the solutions highlighted cutting speed between 170 m/min and 280 m/min, feed ranging from 0.06 mm/rev to 0.10 mm/rev, and depth of cut close to either 0.5 mm or 2.0 mm as the optimal combinations.
- Validation testing revealed relative error values below 10%, supporting the increased accuracy of the model.

5. Limitations and Future Work

The present study does not take into account any dynamic variables such as the vibrations and temperature. Therefore, the model relies purely on continuous variables that cannot capture the sudden changes in the machining state. For these reasons, future work will implement sensory systems that are able to measure the acceleration and temperature changes, with an aim to develop a dynamic prediction system of superior prediction capabilities, by utilizing the appropriate sensors and data acquisition systems. Furthermore, it is anticipated that the dynamic system can become the basis for the development of a digital twin monitoring system.

Author Contributions: Conceptualization, A.T.; methodology, A.T., N.E., K.C. and P.K.; software, A.T.; validation, A.T., N.E., K.C. and P.K.; formal analysis, A.T., N.E., K.C. and P.K.; investigation, A.T.; resources, A.T. and P.K.; data curation, A.T., N.E., K.C. and P.K.; writing—original draft preparation, A.T.; writing—review and editing, A.T., N.E., K.C. and P.K.; visualization, A.T.; supervision, A.T., N.E., K.C. and P.K.; project administration, A.T. and P.K. All authors have read and agreed to the published version of the manuscript.

Funding: This research received no external funding.

Data Availability Statement: Data are contained within the article.

Conflicts of Interest: The authors declare no conflicts of interest.

References

1. Bektaş, B.S.; Samtaş, G. Optimisation of Cutting Parameters in Face Milling of Cryogenic Treated 6061 Aluminium Alloy and Effects on Surface Roughness, Wear, and Cutting Temperatures. *Surf. Topogr. Metrol. Prop.* **2022**, *10*, 025013. [[CrossRef](#)]
2. Balonji, S.; Okokpujie, I.P.; Tartibu, L.K. Parametric Analysis of the Process Performance of Surface Roughness Data of Machined Aluminium Using PSO-ANN. In Proceedings of the icABCD 2021—4th International Conference on Artificial Intelligence, Big Data, Computing and Data Communication Systems, Durban, South Africa, 5–6 August 2021; pp. 1–6. [[CrossRef](#)]
3. Chinchankar, S.; Gharde, S.; Gadge, M. Investigation of Tool Forces, Weld Bead Micro-Hardness and Surface Roughness during Friction Stir Welding of Aluminium 6063 Alloy. *Adv. Mater. Process. Technol.* **2022**, *8*, 231–239. [[CrossRef](#)]
4. Panwar, V.; Kumar Sharma, D.; Pradeep Kumar, K.V.; Jain, A.; Thakar, C. Experimental Investigations and Optimization of Surface Roughness in Turning of En 36 Alloy Steel Using Response Surface Methodology and Genetic Algorithm. *Mater. Today Proc.* **2020**, *46*, 6474–6481. [[CrossRef](#)]

5. Zhang, T.; Yuan, L. Understanding Surface Roughness on Vertical Surfaces of 316 L Stainless Steel in Laser Powder Bed Fusion Additive Manufacturing. *Powder Technol.* **2022**, *411*, 117957. [[CrossRef](#)]
6. Vasanth, X.A.; Paul, P.S.; Varadarajan, A.S. A Neural Network Model to Predict Surface Roughness during Turning of Hardened SS410 Steel. *Int. J. Syst. Assur. Eng. Manag.* **2020**, *11*, 704–715. [[CrossRef](#)]
7. Lakshmana Kumar, S.; Thenmozhi, M.; Bommi, R.M.; Ezilarasan, C.; Sivaraman, V.; Palani, S. Surface Roughness Evaluation in Turning of Nimonic C263 Super Alloy Using 2D DWT Histogram Equalization. *J. Nanomater.* **2022**, *2022*, 9378487. [[CrossRef](#)]
8. Baig, A.; Jaffery, S.H.I.; Khan, M.A.; Alruqi, M. Statistical Analysis of Surface Roughness, Burr Formation and Tool Wear in High Speed Micro Milling of Inconel 600 Alloy under Cryogenic, Wet and Dry Conditions. *Micromachines* **2023**, *14*, 13. [[CrossRef](#)] [[PubMed](#)]
9. Kannan, A.; Mohan, R.; Viswanathan, R.; Sivashankar, N. Experimental Investigation on Surface Roughness, Tool Wear and Cutting Force in Turning of Hybrid (Al7075 + SiC + Gr) Metal Matrix Composites. *J. Mater. Res. Technol.* **2020**, *9*, 16529–16540. [[CrossRef](#)]
10. Bhushan, R.K.; Kumar, S.; Das, S. GA Approach for Optimization of Surface Roughness Parameters in Machining of Al Alloy SiC Particle Composite. *J. Mater. Eng. Perform.* **2012**, *21*, 1676–1686. [[CrossRef](#)]
11. Shanmugavel, R.; Chinthakndi, N.; Selvam, M.; Madasamy, N.; Shanmugakani, S.K.; Nair, A.; Prakash, C.; Buddhi, D.; Dixit, S. Al-Mg-MoS₂ Reinforced Metal Matrix Composites: Machinability Characteristics. *Materials* **2022**, *15*, 4548. [[CrossRef](#)] [[PubMed](#)]
12. John, R.; Lin, R.; Jayaraman, K.; Bhattacharyya, D. Effects of Machining Parameters on Surface Quality of Composites Reinforced with Natural Fibers. *Mater. Manuf. Process.* **2021**, *36*, 73–83. [[CrossRef](#)]
13. Ravikumar, P.; Rajeshkumar, G.; Manimegalai, P.; Sumesh, K.R.; Sanjay, M.R.; Siengchin, S. Delamination and Surface Roughness Analysis of Jute/Polyester Composites Using Response Surface Methodology: Consequence of Sodium Bicarbonate Treatment. *J. Ind. Text.* **2022**, *51*, 360S–377S. [[CrossRef](#)]
14. Altin Karataş, M.; Motorcu, A.R.; Gökaya, H. Study on Delamination Factor and Surface Roughness in Abrasive Water Jet Drilling of Carbon Fiber-Reinforced Polymer Composites with Different Fiber Orientation Angles. *J. Braz. Soc. Mech. Sci. Eng.* **2021**, *43*, 22. [[CrossRef](#)]
15. Slamani, M.; Chafai, H.; Chatelain, J.F. Effect of Milling Parameters on the Surface Quality of a Flax Fiber-Reinforced Polymer Composite. *Proc. Inst. Mech. Eng. Part E J. Process Mech. Eng.* **2024**, *238*, 1537–1544. [[CrossRef](#)]
16. Dixit, N.; Sharma, V.; Kumar, P. Experimental Investigations into Abrasive Flow Machining (AFM) of 3D Printed ABS and PLA Parts. *Rapid Prototyp. J.* **2022**, *28*, 161–174. [[CrossRef](#)]
17. Kechagias, J.D.; Ninikas, K.; Petousis, M.; Vidakis, N. Laser Cutting of 3D Printed Acrylonitrile Butadiene Styrene Plates for Dimensional and Surface Roughness Optimization. *Int. J. Adv. Manuf. Technol.* **2022**, *119*, 2301–2315. [[CrossRef](#)]
18. Juneja, S.; Chohan, J.S.; Kumar, R.; Sharma, S.; Ilyas, R.A.; Asyraf, M.R.M.; Razman, M.R. Impact of Process Variables of Acetone Vapor Jet Drilling on Surface Roughness and Circularity of 3D-Printed ABS Parts: Fabrication and Studies on Thermal, Morphological, and Chemical Characterizations. *Polymers* **2022**, *14*, 1367. [[CrossRef](#)] [[PubMed](#)]
19. Baraheni, M.; Shabgard, M.R.; Amini, S.; Gholipour, F. Experimental Evaluation and Optimization of Parameters Affecting Delamination, Geometrical Tolerance and Surface Roughness in Ultrasonic Drilling of 3D-Printed PLA Thermoplastic. *J. Thermoplast. Compos. Mater.* **2024**, 1–30. [[CrossRef](#)]
20. Gómez-García, D.; Díaz-Álvarez, A.; Youssef, G.; Miguélez, H.; Díaz-Álvarez, J. Machinability of 3D Printed Peek Reinforced with Short Carbon Fiber. *Compos. Part C Open Access* **2023**, *12*, 100387. [[CrossRef](#)]
21. Hassan, M.; Ma, J.; Jahan, M.P. Numerical Modeling and Simulation of Machining of 3D Printed CFRP Composite. *Manuf. Lett.* **2022**, *33*, 415–427. [[CrossRef](#)]
22. Guo, C.; Liu, X.; Liu, G. Surface Finishing of Fdm-Fabricated Amorphous Polyetheretherketone and Its Carbon-Fiber-Reinforced Composite by Dry Milling. *Polymers* **2021**, *13*, 2175. [[CrossRef](#)] [[PubMed](#)]
23. Lv, W.; Qin, X.; Bao, Z.; Guo, W.; Meng, X.; Li, H. Comparison of Joining Hole Making Methods for Fiber Reinforced FDM 3D Printing Parts. *Proc. Inst. Mech. Eng. Part B J. Eng. Manuf.* **2024**, 09544054231223265. [[CrossRef](#)]
24. El Mehtedi, M.; Buonadonna, P.; Loi, G.; El Mohtadi, R.; Carta, M.; Aymerich, F. Surface Quality Related to Face Milling Parameters in 3D Printed Carbon Fiber-Reinforced PETG. *J. Compos. Sci.* **2024**, *8*, 128. [[CrossRef](#)]
25. Cococetta, N.; Jahan, M.P.; Schoop, J.; Ma, J.; Pearl, D.; Hassan, M. Post-Processing of 3D Printed Thermoplastic CFRP Composites Using Cryogenic Machining. *J. Manuf. Process.* **2021**, *68*, 332–346. [[CrossRef](#)]
26. Das, A.; Barrenkala, D.; Debnath, K.; Kumar, P.; Rajan, R.; Patel, S.K. Comparative Assessments of Machining Forces in 3D Printed Polymer Composite during Milling Operation Using Two Coated Carbide End Mills. *Mater. Today Proc.* **2022**, *62*, 6107–6114. [[CrossRef](#)]
27. Alzyod, H.; Ficzer, P. Neosanding Postprocessing for Improving Surface Roughness of Extrusion-Based 3D Printing of PLA Parts: A Comparative Analysis of Stylus Profilometer and Confocal Profilometry Methods. *J. Braz. Soc. Mech. Sci. Eng.* **2024**, *46*, 238. [[CrossRef](#)]

28. Alzyod, H.; Ficzer, P.; Borbas, L. Optimizing Ironing Parameters in Material Extrusion (MEX) Technology: Enhancing Efficiency and Performance. *Discov. Appl. Sci.* **2024**, *6*, 578. [CrossRef]
29. Adak, D.K.; Pal, V.; Das, S.; Ghara, T.; Joardar, H.; Alrasheedi, N.; Haldar, B. Surface Preparation for Coating and Erosion MRR of SS 304 Using Silicon Carbide Abrasive Jet. *Lubricants* **2023**, *11*, 10. [CrossRef]
30. Alam, S.T.; Tomal, A.N.M.A.; Nayeem, M.K. High-Speed Machining of Ti-6Al-4V: RSM-GA Based Optimization of Surface Roughness and MRR. *Results Eng.* **2023**, *17*, 100873. [CrossRef]
31. Equbal, A.; Equbal, M.A.; Equbal, M.I.; Ravindrannair, P.; Khan, Z.A.; Badruddin, I.A.; Kamangar, S.; Tirth, V.; Javed, S.; Kittur, M.I. Evaluating CNC Milling Performance for Machining AISI 316 Stainless Steel with Carbide Cutting Tool Insert. *Materials* **2022**, *15*, 8051. [CrossRef]
32. Neema3D CARBON:PLUS. Available online: <http://www.neema3d.com/main/filaments/ultimate/neema3dt-plus-sign-materials/carbon-plus> (accessed on 20 September 2024).
33. Venkatesh, R.; Kathiravan, S.; Prabhakaran, R.; Ramar, M.; Britto, J.J.J.; Rajakarunakaran, S. *Experimental Investigation on Machinability of Additive Manufactured PLA and PETG Polymers Under Dry Turning Process*; Springer Nature: Singapore, 2022; pp. 553–561.
34. Alzyod, H.; Kónya, G.; Ficzer, P. Integrating Additive and Subtractive Manufacturing to Optimize Surface Quality of MEX Parts. *Results Eng.* **2025**, *25*, 103713. [CrossRef]
35. Dizon, J.R.C.; Gache, C.C.L.; Cascolan, H.M.S.; Cancino, L.T.; Advincula, R.C. Post-Processing of 3D-Printed Polymers. *Technologies* **2021**, *9*, 61. [CrossRef]
36. Tzotzis, A.; Antoniadis, A.; Kyratsis, P. Multivariate Modelling of AA6082-T6 Drilling Performance Using RSM, ANN and Response Optimization. *Int. J. Light. Mater. Manuf.* **2024**, *7*, 531–545. [CrossRef]
37. Daniyan, I.A.; Tlhabadira, I.; Mpofu, K.; Muvunzi, R. Numerical and Experimental Analysis of Surface Roughness during the Milling Operation of Titanium Alloy Ti6Al4V. *Int. J. Mech. Eng. Robot. Res.* **2021**, *10*, 683–693. [CrossRef]
38. Mia, M.; Dhar, N.R. Prediction and Optimization by Using SVR, RSM and GA in Hard Turning of Tempered AISI 1060 Steel under Effective Cooling Condition. *Neural Comput. Appl.* **2019**, *31*, 2349–2370. [CrossRef]
39. Trzepieciński, T.; Szpunar, M.; Kašćák, L. Modeling of Friction Phenomena of Ti-6al-4v Sheets Based on Backward Elimination Regression and Multi-Layer Artificial Neural Networks. *Materials* **2021**, *14*, 2570. [CrossRef] [PubMed]
40. Tzotzis, A.; Tsagaris, A.; Tapoglou, N.; Kyratsis, P. High-Precision CAD-Based Simulation for Turning Considering Tool Microgeometry. *Int. J. Mechatron. Manuf. Syst.* **2023**, *16*, 83–95. [CrossRef]
41. Chen, Y.; Sun, R.; Gao, Y.; Leopold, J. A Nested-ANN Prediction Model for Surface Roughness Considering the Effects of Cutting Forces and Tool Vibrations. *Meas. J. Int. Meas. Confed.* **2017**, *98*, 25–34. [CrossRef]
42. Tzotzis, A.; Nedelcu, D.; Mazurchevici, S.; Kyratsis, P. Surface Quality Evaluation of 3D-Printed Carbon-Fiber-Reinforced PETG Polymer During Turning: Experimental Analysis, ANN. *Polymers* **2024**, *16*, 2927. [CrossRef]
43. El Mehtedi, M.; Buonadonna, P.; El Mohtadi, R.; Aymerich, F.; Carta, M. Surface Quality Related to Machining Parameters in 3D-Printed PETG Components. *Procedia Comput. Sci.* **2024**, *232*, 1212–1221. [CrossRef]
44. Abena, A.; Soo, S.L.; Ataya, S.; Hassanin, H.; El-Sayed, M.A.; Ahmadein, M.; Alsaleh, N.A.; Ahmed, M.M.Z.; Essa, K. Chip Formation and Orthogonal Cutting Optimisation of Unidirectional Carbon Fibre Composites. *Polymers* **2023**, *15*, 1897. [CrossRef] [PubMed]
45. Zeelanbasha, N.; Senthil, V.; Mahesh, G. A Hybrid Approach of NSGA-II and TOPSIS for Minimising Vibration and Surface Roughness in Machining Process. *Int. J. Oper. Res.* **2020**, *38*, 221–254. [CrossRef]
46. Wang, Q.; Jia, X. Optimization of Cutting Parameters for Improving Exit Delamination, Surface Roughness, and Production Rate in Drilling of CFRP Composites. *Int. J. Adv. Manuf. Technol.* **2021**, *117*, 3487–3502. [CrossRef]
47. Geier, N.; Pereszlai, C. Analysis of Characteristics of Surface Roughness of Machined CFRP Composites. *Period. Polytech. Mech. Eng.* **2020**, *64*, 67–80. [CrossRef]

Disclaimer/Publisher’s Note: The statements, opinions and data contained in all publications are solely those of the individual author(s) and contributor(s) and not of MDPI and/or the editor(s). MDPI and/or the editor(s) disclaim responsibility for any injury to people or property resulting from any ideas, methods, instructions or products referred to in the content.